A BEST-ESTIMATE ANALYSIS OF A LOSS-OF-COOLANT ACCIDENT IN A FOUR-LOOP US PWR USING TRAC-PD2*

by

J. R. Ireland
Energy Division
Los Alamos National Laboratory
August 1981

ABSTRACT

A 200-per cent double-ended cold-leg break loss-of-coolant accident (LOCA) in a typical US pressurized water reactor (PWR) was simulated using the Transient Reactor Analysis Code (TRAC-PD2). The reactor system modeled represented a "typical" US PWR with four loops (three intact, one broken) and cold-leg emergency-core-cooling systems (ECCS). The finely noded TRAC model employed 440 three dimensional (r, θ, z) vessel cells along with approximately 300 one-dimensional cells that modeled the primary system loops. The calculated peak-clad temperature of 950 K occurred during blowdown and the clad temperature excursion was terminated at 175 s, when complete core quenching occurred. Accumulator flows were initiated at 10 s, when the system pressure reached 4.08 MPa, and the refill phase ended at 36 s when the lower plenum refilled. During reflood, both bottom and falling film quench fronts were calculated. Top quenching was caused by entrainment from the lower plenum and lower core regions. The entrained liquid was sufficient to form a small, saturated pool (0.3 m deep) above the upper core support plate (UCSP). Also, some of the entrained liquid was carried out the hot legs and vaporized in the steam generators. Strong multidimensional effects were calculated in the reactor vessel, particularly with respect to rod quenching. The calculation shows that some rods located in core regions closest to the intact cold legs (ECCS injection points) quench 125 s sooner than rods located in core regions next to the broken loop.

---

*Work performed under the auspices of the US Nuclear Regulatory Commission

1. INTRODUCTION AND SUMMARY

The Los Alamos National Laboratory has an extensive program, funded and sponsored by the US Nuclear Regulatory Commission (Division of Reactor Safety Research) in the development, assessment, and application of computer methods, specifically the Transient Reactor Analysis Code (TRAC). TRAC is an advanced, best-estimate system code for the analysis of loss-of-coolant accidents (LOCAs) and other thermal-hydraulic transients in light-water reactors (LWRs). TRAC-PD2[1], the latest released version, is designed specifically to analyze LOCA transients in pressurized water reactors (PWRs). TRAC-PD2 employs a three-dimensional (r,θ,z), two-fluid, nonequilibrium, hydrodynamic treatment in the pressure vessel and a one-dimensional, nonequilibrium, drift-flux treatment in the rest of the primary system components. Three-dimensional (3-D) modeling in the vessel is essential to calculate accurately such phenomena as emergency-core-cooling systems (ECCS) bypass in the annular downcomer region, flow distribution from the lower plenum to the core, rod quenching, and asymmetric loop response. TRAC-PD2 calculations[2] of many LOCA-related experiments, such as the Semiscale and the Loss-of-Fluid-Test (LOFT) facility at the Idaho National Engineering Laboratory (INEL), have agreed very well with experimental data, and considerable confidence can be placed in TRAC modeling of the blowdown, refill, and reflood phases typical of PWR LOCAs. This paper discusses the results of a 200-per cent double-ended cold-leg-break LOCA in a typical US PWR performed with TRAC-PD2. This calculation can provide insight into the system's thermal-hydraulic phenomena that occur during the transient, particularly regarding vessel refill and fuel rod quenching. Some important calculated system parameters and vessel multidimensional effects are also presented.

The important conclusions of this analysis are:

1) Peak clad temperature of 950 K occurs during blowdown.
2) ECCS bypass period is calculated from approximately 12 to 36 s during blowdown.
3) Lower plenum refills at 36 s (reflood initiated).
4) Both bottom and falling-film quench fronts are calculated during reflood.

5) A small pool (0.3 m deep) is formed above the upper core support plate (UCSP) from liquid carryover from lower core regions during reflood.
6) Midplanes of all fuel rods are quenched by 130 s.
7) Complete core quenching occurs by 190 s.
8) Core liquid fraction during reflood varies between 25 - 35 per cent because of manometer-type oscillations between the downcomer and core.
9) Strong multidimensional effects are calculated, particularly with regard to rod quenching. That is, some rods located in core regions closest to the intact cold legs quench 125 s sooner than rods located next to the broken loop; this is caused by asymmetric vessel filling.

2. US PWR TRAC MODEL AND STEADY-STATE CALCULATION

2.1. TRAC Input Model

The input model used for the US PWR is essentially the same as reported in Refs. 3 and 4. This model represents a "typical" US four-loop PWR design, which combines features of a variety of different Westinghouse PWR designs.[5-7] Figure 1 shows a schematic of the US PWR primary system used for the TRAC input model. Because the vessel is modeled in three dimensions (r,θ,z), all four loops of the PWR can be modeled explicitly with all of the primary system components such as pipes, tees, accumulators, steam generators, and pumps.

Shown in Fig. 1 is an intact loop that contains the pressurizer (the pressurizer was assumed to be located in an intact loop); another loop, which represents two of the other intact loops (these two loops are modeled separately in the TRAC calculation); and a third loop, which represents the broken loop. Also shown in Fig. 1 are junction numbers (circled numbers) and component numbers (numbers in squares) for a total of 42 components and 45 junctions. As shown in Fig. 1, each of the three intact cold legs includes a tee connected to a FILL that models both the high-pressure injection system (HPIS) and low-pressure injection system (LPIS). The cold legs also include a tee connected to a valve and to an accumulator. There are no ECC systems included in the broken cold leg because it was assumed this system was inoperable and would not affect the transient significantly.

Almost all dimensions for the pipes and tees in each of the loops were obtained from the RELAP input[8] for the BE/EM study[6]. Most of the cells in

the pipes and tees are approximately 1-2 m long, except where geometric considerations forced the use of smaller cells. The HPIS and LPIS are combined into one injection tee connected to a FILL module on each of the three intact cold legs. The actual HPIS and LPIS flow rates, which also were obtained from the BE/EM study,[6] are combined through this tee when these two systems are actuated by trips during the transient. The accumulators are connected to a check valve that opens when the pressure on the loop side of the valve decreases below 4.3 MPa. The pump characteristics such as speed, head, torque, and dimensions also were obtained from Ref. 6.

Figures 2 and 3 show the 3-D noding used for the reactor vessel. Figure 2 shows the axial noding scheme and Fig. 3 shows the horizontal noding scheme.There are 8 angular, 5 radial, and 11 axial nodes, totaling 440 TRAC 3-D cells. This noding distribution was chosen to define the following regions in the vessel: core, upper and lower plena, upper head, barrel-baffle region, and the downcomer. The axial noding corresponds to major flow restriction locations such as the flow distributor plate in the lower plenum, lower core support plate (LCSP), spacer locations in the core, UCSP, and the upper head plate (UHP). The location of the azimuthal nodes accounts for the eight vessel penetrations (four hot legs and four cold legs), while the radial noding accounts for the three major radial power regions in the core and the barrel-baffle and downcomer regions.

The fuel rods extend axially in the core region from the LCSP to the UCSP (levels 4 through 8 in Fig. 2). One lumped average fuel rod representing many actual fuel rods in a given core region (2.248×10^4 W/m core average linear power, 3.028×10^4 W/m peak rod power) is modeled in each core cell (cells 1 through 24 in Fig. 3 - 24 total average rods modeled) for coupling the fuel rod heat transfer to the 3-D vessel fluid dynamics. The total number of fuel rods simulated in the core is 39372 which represents 193 fuel assemblies with 204 fuel rods per assembly (the 15 x 15 array also includes 21 guide tubes). Each radial core region has a different power distribution to simulate an actual radial power profile. The highest relative radial power occurs in the second radial core zone (cells 9 through 16). Eight additional rods also are modeled in selected TRAC cells (cells 1,2,5,6,9,10,13,14 - Fig. 3) to simulate hot rods (3.937×10^4 W/m). In addition to the axial and radial peaking

factors, a hot channel factor of 1.30 is applied to these rods. The hot rods are modeled in the hottest core regions closest to and farthest from the broken cold leg. So, rods 1 through 24 represent the average fuel rods and rods 25 through 32 represent the hot rods. It is important to note that the hot rod calculation is a separate calculation and uses the fluid conditions generated by the average rod core heat transfer. In order to model the conduction from the fuel rod center to the Zircaloy cladding surface, eight radial nodes were used within each rod.

2.2. Steady-State Calculation

Based on the geometry and noding described above, a steady-state calculation was performed to obtain initial conditions prior to the transient. Typical US PWR input parameters[5-7] were used as boundary conditions for the calculation. The steady-state calculation was run to about 300 s of reactor time to assure convergence of all steady-state parameters (e.g. core flow, core ΔT, and steam generator steam conditions). All calculated parameters were in reasonable agreement with available data[5-7], and are representative of "typical" US PWR operating conditions.

3. TRANSIENT CALCULATION

Because this is a "best-estimate" analysis, the following assumptions are made: (1) the plant is operating at rated power (3238 MWt) before the accident; (2) the core is in an equilibrium state; (3) all safety systems (except on the broken loop) are operational throughout the transient; (4) off-site power is maintained throughout the transient, thus the main coolant pumps remain operational; and (5) reactor scram occurs at transient initiation.

From the steady-state results, the transient calculation was initiated with a 200-per cent double-ended cold-leg break in component 1 (Fig. 1). The break was assumed to occur 6.25 m from the reactor vessel outside the biological shield. TRAC BREAK components were used to simulate the containment, and containment pressure history for the transient was taken from the RELAP BE/EM study.[6] The broken cold leg was very finely noded near the break, and the fully implicit solution method in TRAC was used to naturally calculate choked flow. Also at the start of the transient, the secondary sides of all four steam generators were closed to simulate the operation of

isolation valves. Because reactor scram was assumed at transient initiation, the reactor power was tripped and the ANS standard power decay curve was employed.

Table 1 gives a summary of most of the important events during the transient calculation. HPIS flows began at 2 s after break initiation in all three intact loops. Accumulator flows in all intact cold legs began at apprcximately 10 s, when the system pressure had decreased to 4.08 MPa. The first blowdown peak clad temperature of 930 K was reached at 11 s and occurred at the midplane of rod 10. From Fig. 3, rod 10 is located in cell 10 in the highest radial power region closest to the broken cold leg. The blowdown peak temperature at 11 s was due mainly to an adiabatic heatup of the rods. After the peak was reached, the rod temperatures decreased somewhat because of enhanced steam flow through the core. This enhanced steam flow is a result of increased pressure gradients from the core to the downcomer because of localized condensation in the downcomer annulus after the initiation of subcooled accumulator flows at 10 s. ECCS bypass began at 11 s, the pressurizer emptied at approximately 12 s, and most of the saturated fluid expelled from the pressurizer entered the vessel upper plenum and flashed. This fluid provided a significant steam source to the upper portions of the core for cooling. LPIS flows were initiated at 17 s in all intact loops (setpoint - 1.27 MPa); and at approximately 26 s, most of the ECCS bypass ended and refill of the lower plenum began. ECCS bypass occurs when ECCS fluid from the intact loops enters the downcomer annulus and flows azimuthally around the downcomer and out the broken cold leg. The end of bypass is when the upward steam velocity in the inlet annulus of the downcomer decreases sufficiently to allow substantial ECCS liquid penetration. This was calculated to occur at the same time flow reversal occurred in the broken cold leg and flow was drawn in from the containment. As soon as the water height in the lower plenum covered the bottom of the downcomer (downcomer skirt), the steam flow path from the core to the downcomer was blocked and flow stagnation occured in the core.

The fuel rods began heating again at 25 s and at approximately 33 s, which was the end of the blowdown and the beginning of refill, the second peak clad temperature was reached in the same rod as before (rod 10 - 950 K). The

TABLE 1

CALCULATED TABLE OF EVENTS

	Event	Time(s) - Approximate
1.	200 Per Cent Double-Ended Cold-Leg Break (Close off Secondary Side of Steam Generators; Trip Reactor Power)	0
2.	Begin HPIS Flows	2
3.	Accumulator Flows Begin	10
4.	First Peak Clad Temperature Reached - Rod 10 - 930 K - Average Rod	11
5.	Pressurizer Empties	12
6.	Begin LPIS Flows	17
7.	Substantial Amount of ECC Bypass Ends	26
8.	Second Peak Clad Temperature Reached:	
	a. Average Rod - Rod 10 - 950 K	33
	b. Hot Rod - Rod 30 - 1040 K	33
9.	Lower Plenum Refilled and Reflood Begins	36
10.	Accumulators Empty	41
11.	Quench Fronts Move Through Core Midplane - (Min, Max Times)	
	a. Central Region	45 - 90
	b. Middle Region	45 - 130
	c. Peripheral Region	45 - 50
	d. Hot Rods	50 - 150
12.	Entire Core Quenched (Min, Max Times)	
	a. Central Region	60 - 100
	b. Middle Region	75 - 175
	c. Peripheral Region	45 - 70
	d. Hot Rods	90 - 190

temperature of the hot rod in the same cell location (cell 10 - Fig. 3) also peaked at this time (rod 30 - 1040 K). Complete lower plenum refill and the initiation of reflood occurred at 36 s. The accumulators emptied at 41 s, and a slow, gravity reflood process followed using only the LPIS. The midplanes of the peripheral rods (outer core region) quenched first (50 s), followed by the central rods (first radial core region - 90 s), and finally the highest radial power region rods (second radial core region - 130 s). The entire core was quenched by 190 s including the hot rods. A large variation in rod quench times was calculated because of strong multidimensional behavior exhibited in vessel refilling.

3.1 Reactor Vessel Transient Details

The overall cladding temperature time history for the average rods is shown in Fig. 4. This plot represents the maximum cladding temperature calculated for all average fuel rods in the core. This temperature is independent of axial, radial, or azimuthal position. As shown in this plot, the peak temperature of 950 K occurred at the end of blowdown. During reflood, the cladding temperatures decreased an average of 1.5 K/s because of precooling and liquid carryover ahead of the quench front until the cladding temperature reached the minimum stable film boiling temperature (approximately 700 K). All fuel rods, as represented in Fig. 4, were quenched by 175 s.

The cladding temperature time histories for seven core axial positions (bottom of core - 2.97 m; top of core - 7.05 m, core midplane - 5.01 m) of three adjacent average rods (rods 2, 10, 18 in cells 2, 10, 18 - Fig. 3) are shown in Figs. 5 - 7. Figure 8 shows the cladding temperature history for the peak hot rod (rod 30 - cell 10 - 3.937×10^4 W/m). As mentioned previously, the peak clad temperature for both the average and hot rods occurred in rods 10 and 30 (cell 10 - Fig. 3), respectively, during blowdown. Only one hot rod temperature history will be shown (rod 30 located in vessel cell 10) because this rod exhibited the highest calculated cladding temperature (1040 K) and longest quench time of all the rods. The other hot rod temperature histories and quench times (rods 25-32 in cells 1,2,5,6,9,13,14) were similar to the average rods calculated in the same cells (rods 1,2,5,6,9,13,14). Rods 2, 10 and 18 were calculated to be the hottest average rods for each radial power region. These rods are located in cells closest to the broken cold leg (Fig. 3). These rods were the hottest because of asymmetric core refilling

during reflood. The core cells closest to the intact cold legs (ECCS injection points) received more ECCS fluid than those cells next to the broken cold leg as there was no ECCS on the broken loop. The asymmetric core quenching is evidenced by comparing the cladding temperature history in Fig. 6 to Fig. 9. Figure 9 shows an average rod temperature history for rod 14 (cell 14 - Fig. 3), which is in the same radial power region as rod 10, and is located directly across from rod 10 in a cell adjacent to an intact cold leg (refer to Fig. 3). From this comparison it is obvious that more liquid penetrated the core in cells closest to the intact cold legs. Another major contributor to the large differences in cladding temperature response between rods 10 and 14 was large differences (factors of 10-50) in liquid and steam flow rates during blowdown in these cells. During blowdown, circulation patterns were established in the core region during the ECCS bypass period; and strong co-current downflow was calculated in cells closest to the intact loops while small, co-current upflow was calculated in cells next to the broken loop. These large differences in the flow rates caused large differences in the heat transfer coefficients that determined the cladding temperatures.

The effects of subcooled ECCS injection and ECCS bypass are important during the blowdown and refill phases of the calculation. Figure 10 shows the lower plenum liquid volume fraction as a function of time. Figure 11 shows the upper plenum average pressure for the entire transient. Figure 11 shows that the blowdown phase ended at approximately 26 s. It is at this time that ECCS bypass ended and refill began. This is evidenced by the refill of the lower plenum (Fig. 10) shortly after this time. Table 1 shows that accumulator flows were initiated at 10 s (4.08 MPa - Fig. 11) after the break and at this point the liquid fraction in the lower plenum was about 20 per cent (Fig. 10). This liquid fraction decreased and leveled off at about 15 per cent until about 26 s after the break. At this time ECCS bypass ended. Figure 12, which shows the average saturation and liquid temperatures in the lower plenum, also graphically illustrates this bypass phenomenon. As can be seen from this figure, there was little subcooled ECCS liquid penetration into the lower plenum from about 11 to 26 s as evidenced by equal liquid/saturated fluid temperatures. After this point, the subcooled ECCS liquid began to penetrate the downcomer annulus and refill the lower plenum. After the

accumulators emptied at approximately 41 s, the amount of subcooling in the lower plenum decreased because only the LPIS was available after this time.

To illustrate further the bypass, refill, and reflood phases of the transient, the downcomer and core liquid volume fractions are shown in Figs. 13-14. As mentioned previously, the accumulator flows were initiated at 10 s and ended at 41 s. Also, ECCS bypass occurred from 11 s until 26 s. The downcomer liquid volume fraction (Fig. 13) reached a minimum level at 10 s, then filled slightly after the accumulator water reached the downcomer annulus (11 s). However, because of partial ECCS bypass, the downcomer did not fill. At the end of bypass, the downcomer filled rapidly and remained almost full until the accumulators began to empty (35 s). During this time the lower plenum filled (Fig. 10), but the core remained essentially dry (Fig. 14). As soon as the lower plenum filled the downcomer head was large enough to force a large slug of liquid into the core (Fig. 14). This slug quenched the lower core regions rapidly and caused a gradual pressure rise in the core (Fig. 11) as a result of nucleate boiling. This slug of liquid boiled off rapidly; however, the pressure rise due to the boiling was gradual so that the lower plenum did not empty (Fig. 10).

In comparing the blowdown phase and time-to-lower-plenum refill of the US PWR calculation to the LOFT facility (LOFT test L2-3 - L2-3 is used because the peak power is the same as the US PWR calculation--39.4 kW/m)[9], it is seen that the initial blowdown periods are quite similar and the time-to-lower-plenum refill is essentially the same (US PWR - 36 s; LOFT L2-3 - 35 s). This implies that the ECC bypass periods are about the same as well as the later stages of blowdown and refill. The differences in the blowdown histories can be attributed to two important points.

1. Initial system pressure - The steady-state pressure for the US PWR calculation was 15.51 MPa compared to 15.06 MPa for LOFT test L2-3. Therefore, the subcooled blowdown period is longer for the US PWR calculation causing a longer period for higher break flow which results in a shorter blowdown period.

2. Rod quenching - In L2-3, some rods experienced alternate periods of dryout and quenching during blowdown. The quenching of some of the rods during blowdown contributed to holding the pressure up as a result of an increase in vapor generation in the core. Quenching during blowdown was not calculated for the US PWR, thus the system pressure continued to decrease.

Overall, in comparing general trends during blowdown and refill for LOFT L2-3 to the US PWR calculation, the results appear quite reasonable, especially with regard to the length of blowdown, ECCS bypass period, and time-to-lower-plenum refill.

After the accumulators emptied, the downcomer began emptying slowly (Fig. 13) and the core gradually filled (Fig. 14), typical of a gravity reflood process. During reflood the downcomer head from the LPIS was balanced by the core boiling rate and the loop resistance, causing a manometer-type situation. If the peaks and valleys of the oscillations during reflood are compared, the liquid volume fractions are out of phase with a period of 3-6 s. These oscillations were compared to those exhibited in the Primarkreislaufe (PKL) system reflood tests[10]; and the period of the manometer oscillations calculated by TRAC and those of the PKL tests were very similar.

It appears from the US PWR downcomer liquid volume fraction plot (Fig. 13) that the downcomer is approximately 45 per cent full during reflood. There needs to be some clarification as to what this plot means. This plot represents the amount of liquid in the downcomer as defined in TRAC. TRAC assumes the downcomer extends from the bottom of the downcomer skirt to the top of the downcomer (axial levels 3 through 10 in Fig. 2), and does not include that portion of the downcomer below the skirt. Therefore, to obtain the actual downcomer collapsed water level at 170 s using Figs. 2 and 13,

$$h_{DC} = 0.45(10.82 - 2.496) + 2.496 = 6.24 \text{ m} \qquad (1)$$

where

h_{DC} = downcomer collapsed water level.

The 2.496 m is the distance from the bottom of the lower plenum to the downcomer skirt, and the 10.82 m is the top of the downcomer. So, at 170 s the downcomer water level is approximately 0.75 m below the height of the upper core support plate (axial level 8 in Fig. 2), which translates to an actual downcomer liquid volume fraction of about 0.60. If the top of the downcomer is defined to be the height to the bottom of the cold leg (approximately 8.0 m for the US PWR), which really represents a "full" downcomer, then the actual downcomer liquid volume fraction is approximately 0.8.

From representative Cylindrical Core Test Facility (CCTF) experiments[11], it is seen that the downcomer collapsed water level during reflood is approximately 6.0 m, which is equivalent to the height of the upper core support plate for this test facility. Therefore, if the effects of scale, downcomer wall heat transfer, etc. are considered, the collapsed downcomer water level height calculated for US PWR (6.2 m) compares very well with that measured in CCTF (6.0 m).

As discussed previously, the core completely quenched by 190 s. However, the core liquid fraction was only about 25 - 30 per cent during reflood (Fig. 14). The core quenched completely as a result of liquid entrainment and carryover from the lower core regions during reflood; as a result, a substantial amount of precooling and falling film quench front motion occurred. Large, experimental reflood tests for large-break reflood and cold-leg ECCS injection such as the CCTF[11] and PKL (Appendix C of Ref. 10) show that both falling films and bottom reflood quench motion are observed experimentally with a core liquid fraction typically 30-40 per cent. Considering the effects of scaling and differences in the experimental facility design when compared to a full scale PWR, the agreement is quite remarkable between the experimentally observed core liquid fraction and rod quenching behavior and the TRAC US PWR calculation.

Figure 15 shows a plot of the upper plenum liquid volume fraction. During blowdown, the upper plenum emptied, but during reflood the liquid fraction slowly increased as a small, saturated pool formed above the UCSP. The pool depth varied approximately linearly from 0.0 m at t = 30 s to 0.3 m at t = 190 s. It should be noted that pool formation of similar height was observed in CCTF Test 010[11], which simulated a double-ended cold-leg break

with cold-leg ECCS injection. Using the definition of carryover rate fraction (CRF), as defined in the Code of Federal Regulations[12] (10CFR50, Appendix K), an estimate of the amount of liquid carryover from the core to the upper plenum was made. The CRF is defined as

$$CRF = \frac{\text{Core exit liquid flow rate}}{\text{Core inlet liquid flow rate}} \qquad (2)$$

Figures 16 and 17 show the core inlet and core exit liquid flow rate histories, respectively, as calculated by TRAC. Some oscillatory behavior is evident, especially in the core inlet liquid flow because of the manometer oscillations between the core and downcomer discussed previously. During reflood, the core inlet liquid flow rate varied approximately between 250 - 500 kg/s on the average (Fig. 16). The core exit liquid flow rate (Fig. 17) was more stable than the core inlet flow, and varied approximately from 100 to 200 kg/s during reflood. Substitution of these values of inlet and exit liquid flow rates into the CRF equation (Eq. 2) gives the maximum and minimum carryover rates during reflood of

$$(CRF)_{MIN} = \frac{100}{500} = 0.2 \qquad (3)$$

and,

$$(CRF)_{MAX} = \frac{200}{250} = 0.8 \qquad (4)$$

So, on the average, the CRF varies between 0.2 and 0.8 (average of about 0.5) during reflood. This implies that between 20 and 80 per cent of the ECCS water entering the core is carried through to the upper plenum at a given time. Therefore, a good cooling mechanism is provided for the upper core regions during reflood and it is this heat transfer mechanism that allows for good precooling and falling-film quench front motion.

To see if the CRF and upper plenum pool formation calculated by TRAC are reasonable, the Full-Length Emergency-Cooling-Heat-Transfer (FLECHT) Facility Test 4831[13] was investigated. FLECHT test 4831 used an axial cosine power

distribution and a core flooding rate of 1.5 in/s. For comparison, the minimum core average flooding rate (FR) for the US PWR calculation, using Fig. 16 for the core inlet liquid flow rate, a density of 930 kg/s, and the core flow area of about 6.0 m^2 yields:

$$(FR)_{MIN} = \frac{\dot{m}}{\rho . A} = \frac{250}{930.6} = 0.04 \text{ m/s} = 1.8 \text{ in/s}. \quad (5)$$

This flooding rate compares reasonably well with FLECHT Test 4831.

The experimental results for test 4831 show that for a core inlet liquid flow rate of 0.5 kg/s, the effluent liquid mass flow rate varies from about 0.25 to 0.4 kg/s giving a CRF (Eq. 2) of 0.5 to 0.8 (maximum). Therefore, the core flooding rate and CRF for FLECHT Test 4831 compare reasonably well (considering the effects of scale, etc.) with the FR and CRF of the TRAC US PWR calculation. Thus, the reflood and entrainment models used in TRAC are acceptable and applicable to full-scale PWRs. However, results might be improved further by use of a separate droplet field to obtain more accurate axial void distributions in the upper core regions and upper plenum above the pool.

Figure 18 shows the vessel liquid mass inventory as a function of transient time. During blowdown, the vessel emptied rapidly until accumulator flows were initiated at 10 s. The vessel inventory reached its minimum value at this time (8000 kg). The vessel inventory remained at about this value during the bypass period, then at the end of bypass (26 s), the vessel began filling essentially at the same rate as the lower plenum filling rate (Fig. 10). The vessel filled to slightly over 50 per cent (50000 kg) by about 40 s, which corresponds to the end of accumulator flow. As discussed previously, a slug of water entered the core and was boiled off soon after 40 s, with a gradual increase in core pressure. The partial core filling and boiling at this time is shown in Fig. 18. After the accumulators emptied, the LPIS was the only source of water to the vessel. After 50 s the vessel inventory increased only slightly as a balance was obtained between the LPIS flow and the core boiling rate as a result of rod quenching during reflood.

3.2. Intact Loop(s) Transient Details

Because all four primary loops are modeled separately in the calculation (Fig. 1), differences in loop response were calculated. These differences existed because of (1) differences in loop geometry (that is, pressurizer located in one loop only, cold-leg break in another loop, etc.), and (2) multidimensional behavior in the vessel. Differences in the response of the intact loops existed mainly between the loop containing the pressurizer and the other two intact loops. The intact loops that did not contain the pressurizer exhibited very similar transient behavior.

The accumulator response for each of the three intact cold legs during refill was very similar even though a separate accumulator was modeled on each loop. Figure 19 shows the accumulator mass flow rate (negative flow is into cold leg) during the transient. This figure shows that accumulator flow was initiated shortly after 10 s and the flow terminated by 41 s. The accumulator flow rate peaked at 1800 kg/s (maximum ΔP at approximately 15 s) then degraded and finally emptied as the pressure differential across the discharge nozzle decreased.

In an actual PWR system, nitrogen cover gas is used above the accumulator liquid to maintain the setpoint pressure. When the accumulator empties, the nitrogen is expelled into the primary system. The major effect of the nitrogen would be to reduce the condensation efficiency in the cold legs and downcomer region, thus affecting the calculation of end-of-ECCS bypass to some extent. Future versions of TRAC will model noncondensible gases, thus the effects of nitrogen on condensation efficiency can be addressed at that time.

Figure 20 shows a plot of the HPIS-LPIS flow rate into an intact cold leg (negative flow is into cold leg). The HPIS-LPIS flow is modeled as a function of system pressure to simulate the actual response of the LPIS centrifugal pumps. The LPIS flows began at approximately 15 s and reached maximum flow by about 33 s. Again, similar response was calculated for the other two intact loops. The maximum LPIS flow into each intact cold leg was about 66 kg/s for a total LPIS flow of 200 kg/s. Although the actual LPIS capacity of typical US PWRs is roughly twice this value, full credit cannot be taken because in most designs the LPIS injection ports are tied by a common crossover that connects the intact and broken loops. Thus, a flow split would occur between

the intact and broken loops and a significant amount of LPIS flow (depending upon the pressure differential between the loops) would go to the broken loop and out the break.

The LPIS flow used in the US PWR calculation compares well with the scaled LPIS flow used in experimental test facilities such as CCTF[11], FLECHT[13], and the LOFT facility.[9] These comparisons are shown in Table 2 for similar tests.

TABLE 2
LPIS FLOW COMPARISONS

Facility	Scaled Flow (kg/s)	Scaling Factor[a]	Scaled-Up Flow (kg/s)
1. US PWR	-----	-----	200
2. CCTF-Run 010	8.4	21.4	180
3. FLECHT-Test 4831	0.5	437.5	220
4. LOFT-Test L2-3	6.0	30.0	180

[a]Scaling based on number of rods

Figures 21 and 22 show the void fraction and mass flow rate respectively for an intact loop cold leg at the vessel junction (cold leg 2 - refer to Fig. 1 for identification). Positive flow is defined as flow into the vessel. Similar void fraction and flow rate response are exhibited in the other intact loops. Figure 21 shows that the cold legs voided quite rapidly after break initiation and the void fraction increased until accumulator flows were initiated at about 10 s. Conversely, the cold leg flow rate steadily decreased (Fig. 22) after break initiation and decreased until the start of accumulator flow. Between 10 and 40 s, a significant amount of slugging (condensation oscillations) was calculated because of condensation in the steam-filled cold legs. After the accumulators emptied (40 s), the slugging ceased because the amount of subcooled ECCS water entering the cold legs reduced to only the LPIS injection rate (66 kg/s per loop). During reflood, the calculated void fraction and mass flow rate in the cold legs were very stable with no evidence of slugging.

Figures 23 and 24 show the void fraction and mass flow rate respectively for an intact loop hot leg at the vessel junction (hot leg 13 - refer to Fig. 1 for identification). Again, the sign convention for positive flow is into the vessel. The hot legs voided soon after break initiation and remained essentially void for the entire transient. After 100 s, some minor oscillations in void fraction occurred (Fig. 23) as entrained liquid from the core passed during reflood through the upper plenum and out the hot legs. As discussed previously, most of this entrained liquid formed a pool above the UCSP, but a small amount of liquid (especially from the outer core cells) escaped the pool and left the vessel out the hot legs. The void fractions in the hot legs after 100 s typically ranged from 0.97 - 0.99, indicating a very small amount of entrained liquid. This liquid passed from the hot legs to the steam generators and was then vaporized as a result of secondary-to primary-side heat transfer. This "reverse" heat transfer mechanism occurred because the steam generator secondary sides were isolated at break initiation (Table 1), and after the primary side had blown down to a pressure below the secondary side (5.8 MPa), secondary-to primary-side heat transfer occurred. As a result of the vaporization of the entrained liquid on the primary side, local increases in pressure occurred. If these pressure increases are relatively large compared to the core pressure, then steam-binding will result, causing a back-pressure on the core and retarding the core flooding rate. However, because such a small amount of liquid was vaporized in this calculation, the pressure increase was insignificant compared to the boiling rate in the core during reflood. Thus, no evidence of steam-binding was calculated to occur. As discussed previously, the addition of a separate droplet field in the vessel and pipe components might alter these results such that "steam-binding" might become important.

Figure 24 shows that flow was predominantly from the vessel to the hot leg (positive flow into vessel) for most of the transient. This is because the pressure gradient was always from the vessel upper plenum to the downcomer as a result of boiling in the core and condensation in the cold legs at the ECCS injection locations. The flow rate in the hot legs during reflood was quite small compared to the cold legs because the hot legs were essentially steam-filled. The small perturbations in flow rate in the hot legs were a result of the liquid entrainment discussed above.

The hot-leg response for the other intact hot leg (hot-leg 14 - Fig. 1) without the pressurizer was very similar to hot-leg 13. However, for the intact hot leg that includes the pressurizer (hot-leg 15 - Fig. 1), the response was quite different, at least for the blowdown phase of the transient. Figure 25 shows the mass flow rate at the vessel junction for hot-leg 15. Although there was not much difference in the void fraction response, the mass flow rate at the vessel junction (Fig. 25) was quite different from hot-leg 13 (Fig. 24). The mass flow rate for hot-leg 15 was positive (into the vessel) for the first 15 s because of saturated flow from the pressurizer to the hot leg through the pressurizer surge line. Table 1 shows that by 12 s the pressurizer emptied and this corresponds approximately to the time that positive flow from hot-leg 15 to the vessel (Fig. 25) ceased. After about 15 s, the flow rate and void fraction calculated for hot-leg 15 were very similar to the other intact hot legs. The surge of pressurizer water into the vessel before 15 s aided somewhat in early quenching from the top of the core of rods in cells associated with hot-leg 15 (rods 8, 16, 24 - Fig. 3). However, the main advantage of this flow was to provide additional steam for cooling the upper core regions during the first 15 s of the transient, as discussed in Section 3.0.

Therefore, although the intact cold-leg responses are quite similar during the transient, the responses of the intact hot legs are different (at least for the first 15 s), primarily due to the pressurizer. During reflood, the hot-leg behavior is similar for all the intact loops, and a small amount of liquid entrainment from the vessel out the hot legs is calculated.

3.3. Broken-loop Transient Details

The broken loop consists of the broken cold leg (component 1 - Fig. 1), pump, steam generator and hot leg (component 12 - Fig. 1). As discussed previously, no ECC systems were modeled in the broken loop. The broken ends of the cold leg were connected to BREAK components that simulated the containment.

Some of the broken cold-leg details are shown in Figs. 26 and 27. The vessel-side-break mass flow rate out the broken cold leg into the containment is shown in Fig. 26 (positive flow into containment). The broken cold leg void fraction plot (Fig. 27) graphically illustrates the ECCS bypass period from 11 to 26 s. During this time, the void fraction decreased to about 0.5

as a result of accumulator water bypassed azimuthally around the downcomer and out the broken cold leg. Then, at 26 s when bypass ended, the void fraction increased instantaneously to 1.0 as a result of flow reversal in the broken cold leg. This flow reversal was caused by local depressurization in the downcomer annulus as a result of condensation from the highly subcooled accumulator water. This causes the pressure drop in the broken cold leg to be from the containment to the vessel, thus the flow reversed and steam was drawn in from the containment (no air field is modeled in TRAC-PD2). As the accumulators emptied, the magnitude of this adverse pressure gradient decreased, and at about 37 s, the flow direction changed again in the broken cold leg from the vessel to the containment. When this occurred, some liquid was again carried out the broken cold leg because of partial bypass of the remaining accumulator flow and the LPIS.

Figure 28 shows the void fraction in the broken loop hot leg (hot-leg 12 Fig. 1) at the vessel junction. The flow rate out the broken-loop hot-leg side is shown in Fig. 29 (positive flow into containment). A comparison of the void fraction and mass flow rate out the hot-leg side of the break to the corresponding parameters of the intact-loop hot legs (Figs. 23 and 24) shows that differences existed only during the blowdown phase of the transient. The broken-loop hot leg voided sooner and the mass flow rate was substantially higher than the intact loops during blowdown. However, for the remainder of the transient, the void fraction and flow rate were comparable to the intact loops; and entrainment was calculated from the vessel out the broken-loop hot leg that is similar to the intact hot legs.

In comparing the US PWR broken cold-leg response to that of CCTF during reflood, it is seen that the responses are quite similar. Figure 30 shows the US PWR broken cold-leg break flow (positive flow into containment) during reflood. It is seen that a large amount of the injected LPIS flow (200 kg/s) is bypassed during the entire reflood phase (on the average of 50-60 per cent). Recent analysis of CCTF Test C1-11[14], which is similar to CCTF-Run 010[11], shows that approximately 50 per cent of the LPIS injection flow (which scales up approximately to the 200 kg/s used in the US PWR calculation--Table 2) is bypassed during reflood. One reason for the similar responses is similar downcomer water levels, as discussed in Section 3.1.

In Fig. 3, the broken loop is connected to vessel cells 25 (broken hot leg) and 34 (broken cold leg). These cells communicate with core cells 1, 2, 9, 10, 17, and 18. As discussed previously, the calculation shows that rod temperatures and quenching in cells associated with the broken loop have the highest cladding temperatures and latest quench times (refer to Figs. 5 - 9). The main reason for this, again, is asymmetric core filling as a result of no ECC systems modeled in the broken loop. Rods located in core cells associated with the intact cold legs (ECCS injection locations) farthest from the broken loop are the first to quench, and have the lowest cladding temperatures.

4. SUMMARY AND CONCLUSIONS

The results of this calculation demonstrate some important points about the use and applicability of TRAC to large-break LOCA calculations of full-scale PWRs. TRAC is capable of performing this calculation in a single, continuous pass from blowdown through reflood. The overall results are quite reasonable, and compare both qualitatively and in some instances quantitatively (for example, core flooding rate, carryover rate, and upper plenum pool formation) with available experimental data. Strong evidences of multidimensional behavior are calculated, particularly with regard to asymmetric vessel refilling and fuel rod quenching. Some rods located in core regions closest to the intact cold legs quench 125 s sooner than rods located in core regions next to the broken loop. The 3-D TRAC modeling of the reactor vessel is essential for this type of transient to calculate such phenomena as ECCS bypass in the annular downcomer region, flow distribution in the core during refill, multidimensional rod quenching, and asymmetric loop response.

Some of the TRAC modeling deficiencies that may affect large-break LOCA calculations of this type include the lack of a separate droplet field in the vessel and in the one-dimensional components, and a non-condensible gas field. The addition of a droplet field may improve core heat transfer during reflood, subcooled pool formation in the upper plenum, and entrainment out the hot legs. Addition of a noncondensible gas field will allow the effects of nitrogen injection from the accumulators on condensation efficiency to be calculated and air to be modeled in the containment.

In conclusion, this calculation has provided insight into the system thermal-hydraulic phenomena for a postulated full-scale PWR large-break LOCA, and hopefully will lead to calculations that will resolve some important PWR safety questions.

REFERENCES

1. "TRAC-PD2: An Advanced Best-Estimate Computer Program for Pressurized Water Reactor Loss-of-Coolant Accident Analysis," Los Alamos National Laboratory report LA-8709-MS (April 1981).

2. "TRAC-PD2 Developmental Assessment," Los Alamos National Laboratory report (to be published).

3. J. F. Jackson and M. G. Stevenson, "Nuclear Reactor Safety Quarterly Progress Report, October 1 - December 31, 1977," Los Alamos National Laboratory report LA-7195-PR (April 1978).

4. J. F. Jackson and M. G. Stevenson, "Nuclear Reactor Safety Quarterly Progress Report, January 1 - March 31, 1978," Los Alamos National Laboratory report LA-7278-PR (June 1978).

5. Commonwealth Edison Company, "Zion Nuclear Power Station, Unit 1, Startup Test Report," Docket No. 50-295, License No. DPR-39 (November 1974).

6. G. W. Johnson, F. W. Childs, and J. M. Broughton, "A Comparison of Best-Estimate and Evaluation Model LOCA Calculations: The BE/EM Study," Idaho National Engineering Laboratory report PG-R-76-009 (December 1976).

7. Westinghouse Nuclear Energy Systems, "Reference Safety Analysis Report," RESAR 41 (December 1975).

8. "RELAP4/MOD5 User's Manual - Volume II," Idaho National Engineering Laboratory report ANCR-NUREG-1335 (September 1976).

9. P. G. Prassinos, B. M. Galusha, D. B. Engelman, "Experiment Data Report for LOFT Power Ascension Experiment L2-3," EG&G Idaho, Inc. report NUREG/CR-0792, TREE-1326 (July 1979).

10. B. Brand, R. Kirmse, F. Winkler, "Specification: German Standard Problem No. 2: Refill and Reflood of a Pressure Vessel with Simulated Primary Loops (PKL)," Kraftwerk Union report, July 1978, translated to English, Los Alamos National Laboratory report LA-TR-77-44 (February 1975). Also, Appendix C, "Selected Test Results from the K5.3a Experiment of the PKL-IA Test Series" (January 1979).

11. K. Hirano, J. Sugimoto, and K. Sekiguchi, "Quick-Look Report on Large Scale Reflood Test-1 CCTF Test C1-1 (Run 010)," Japan Atomic Energy Research Institute memo 8453 (August 1979).

12. 10CFR Part 50, "Acceptance Criteria for Emergency Core Cooling Systems for Light-Water Cooled Nuclear Power Plants," Federal Register, Vol. 39, No. 3 (January 1974).

13. E. R. Rosal, "FLECHT Low Flooding Rate Cosine Test Series Data Report," Westinghouse Electric Co. report WCAP-8651 (1975).

14. R. K. Fujita, "Analysis of CCTF Core 1 Test C1-11 (Run 20) Data," Los Alamos National Laboratory Technical Note LA-2D/3D-TN-81-13 (April 1981).

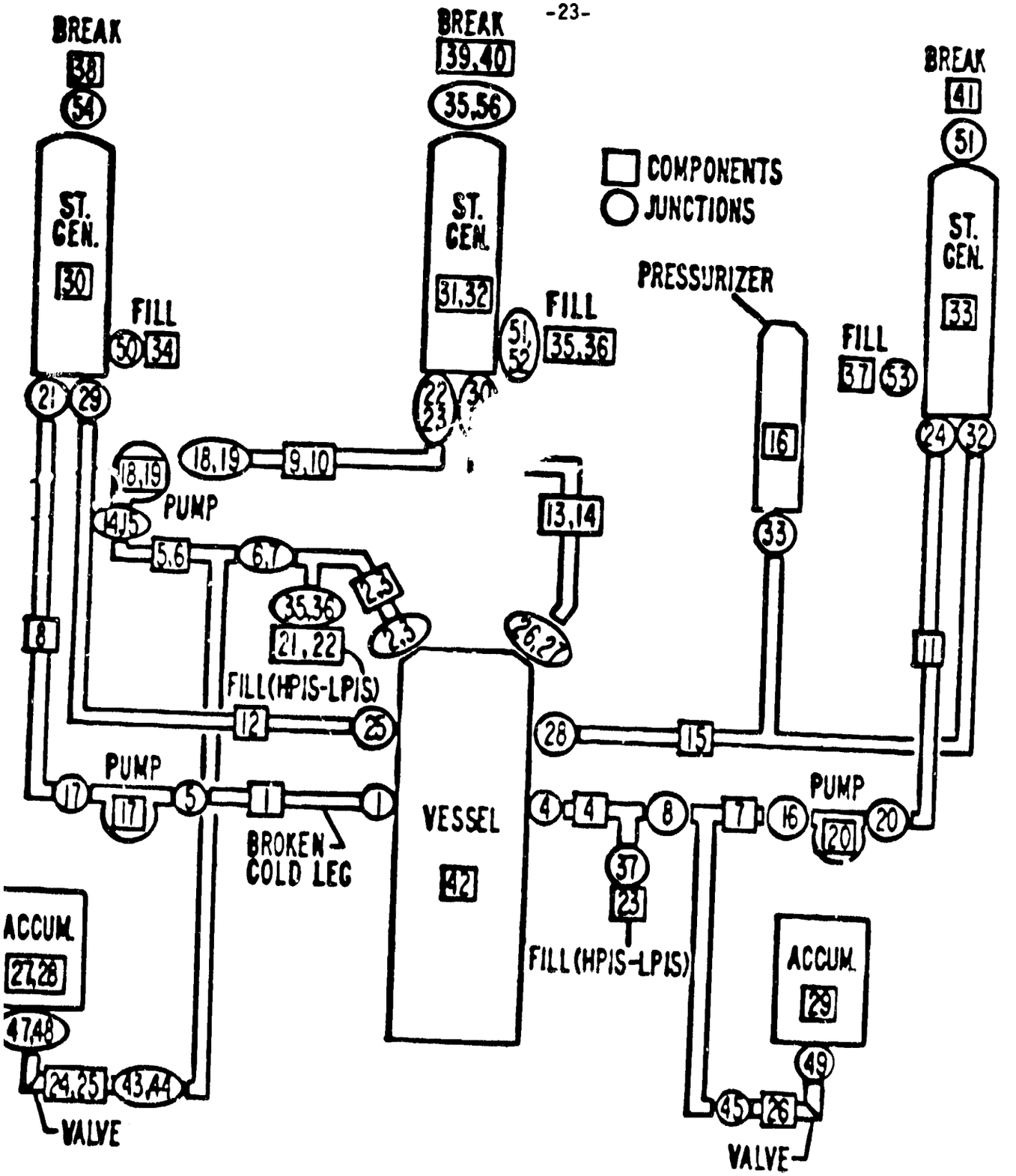

Figure 1. Typical US PWR TRAC schematic.

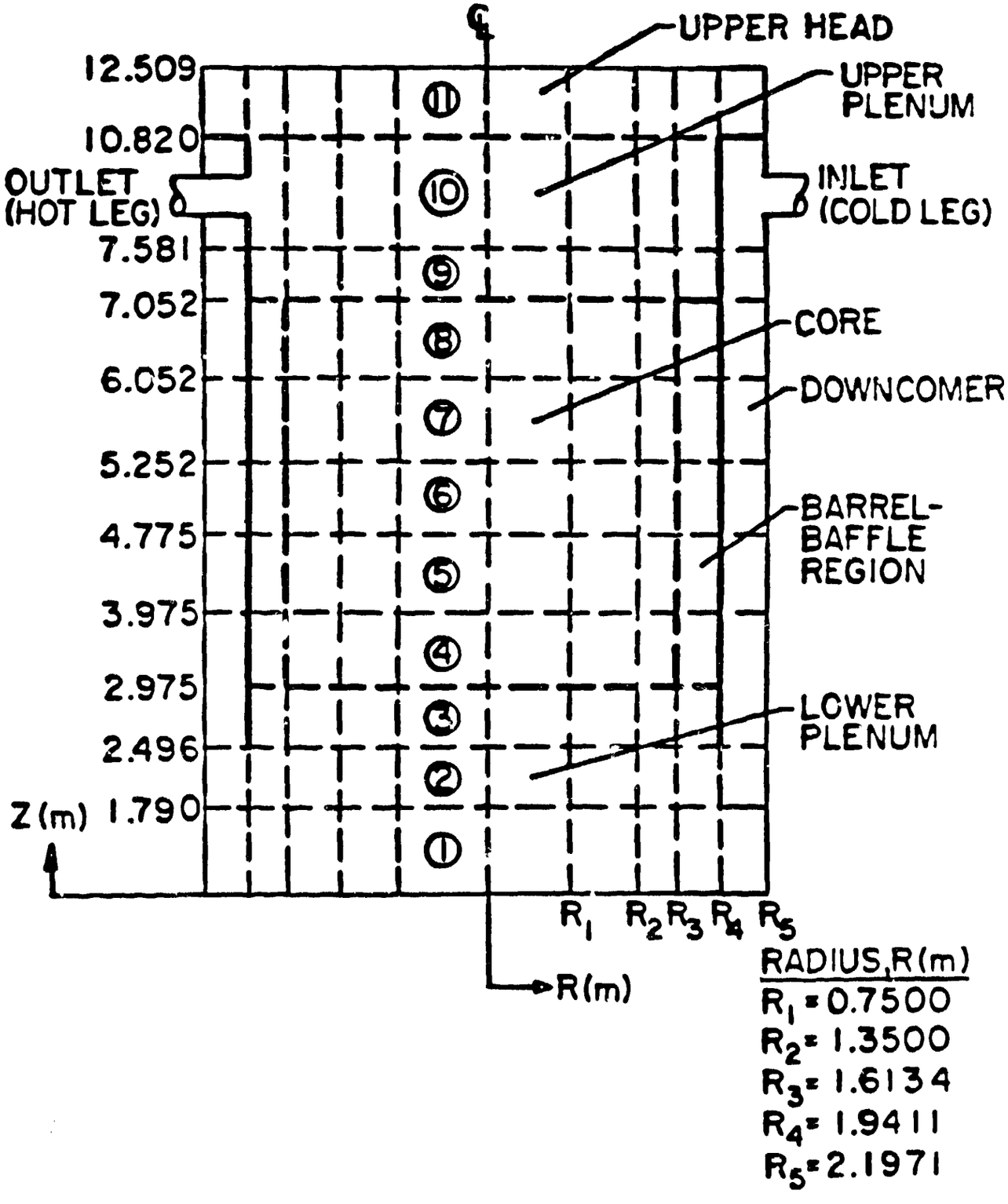

Figure 2. Vessel axial noding.

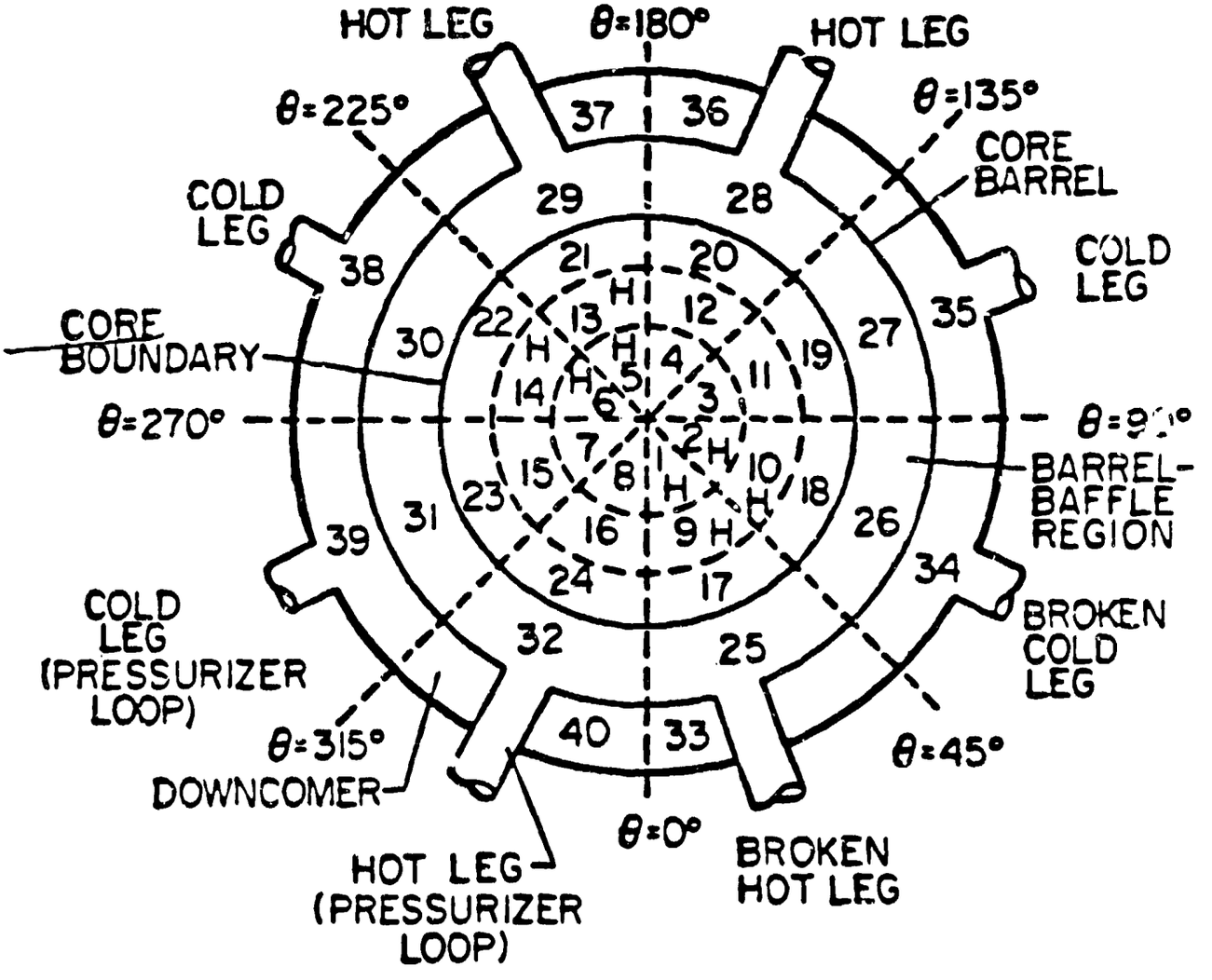

Figure 3. Vessel horizontal noding.

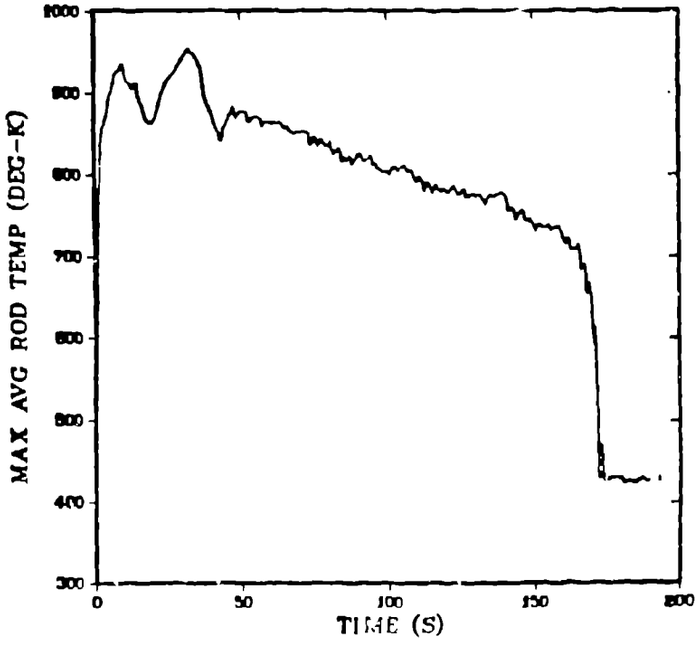

Figure 4. Maximum average rod temperature history.

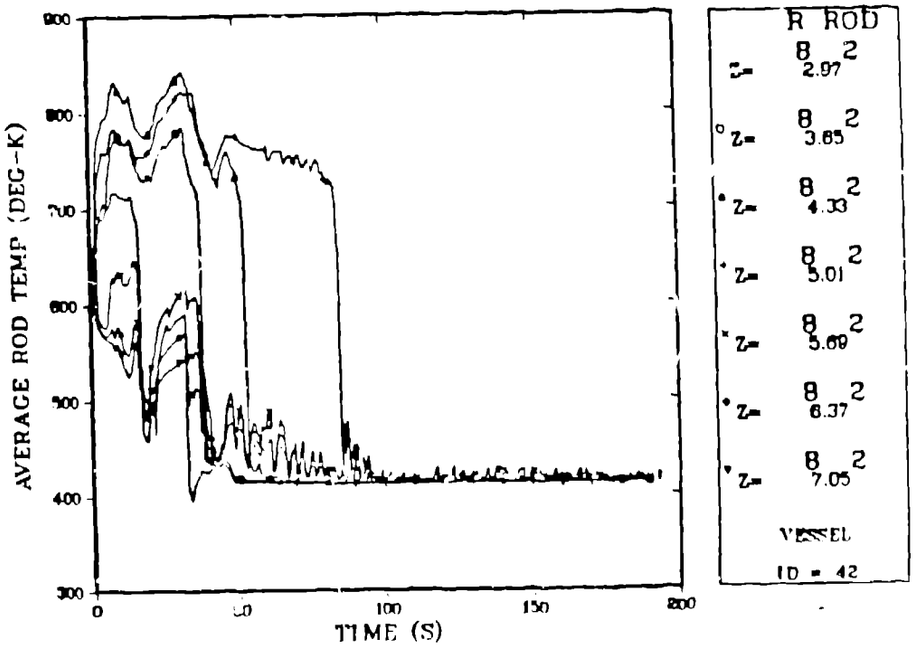

Figure 5. Rod 2 average rod cladding temperature history.

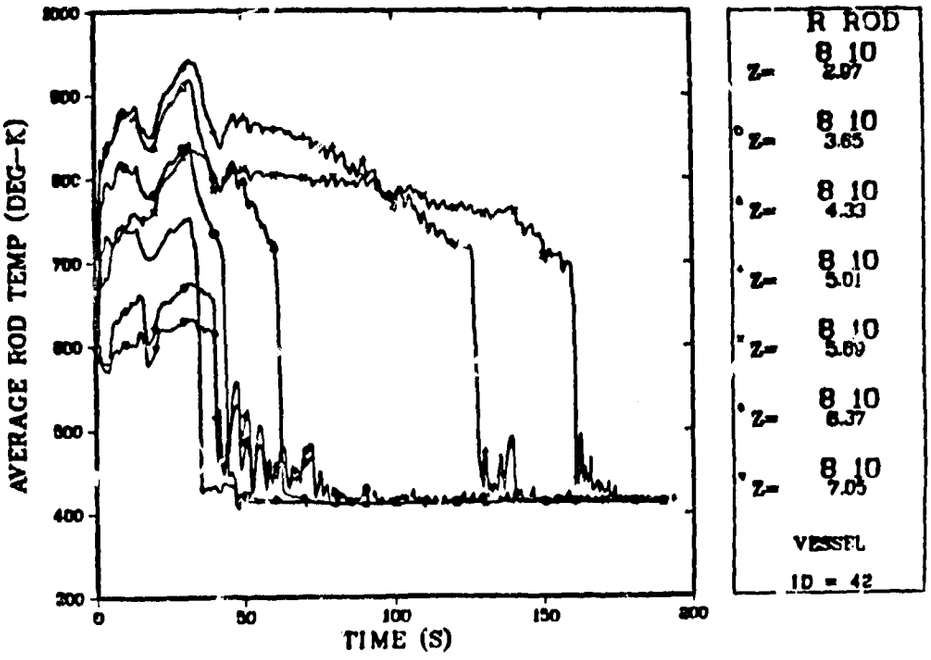

Figure 6. Rod 10 average rod cladding temperature history.

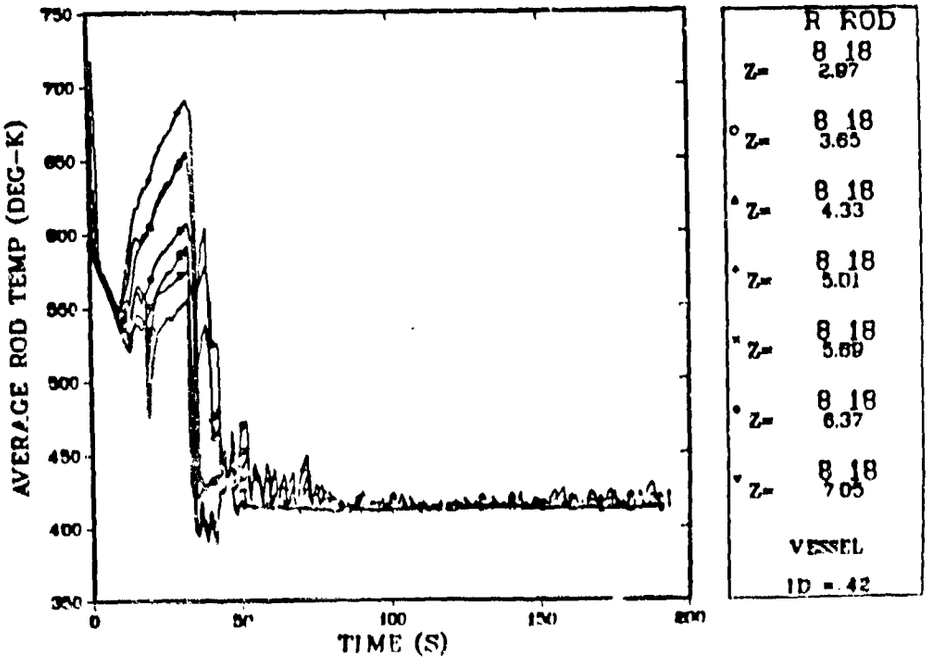

Figure 7. Rod 18 average rod cladding temperature history.

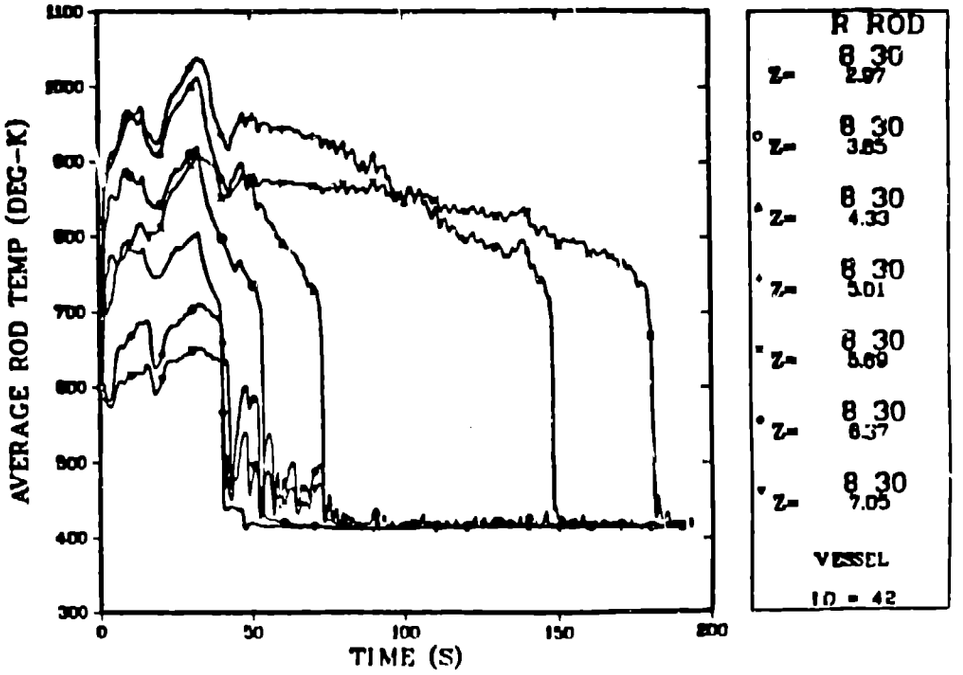

Figure 8. Rod 30 hot rod cladding temperature history.

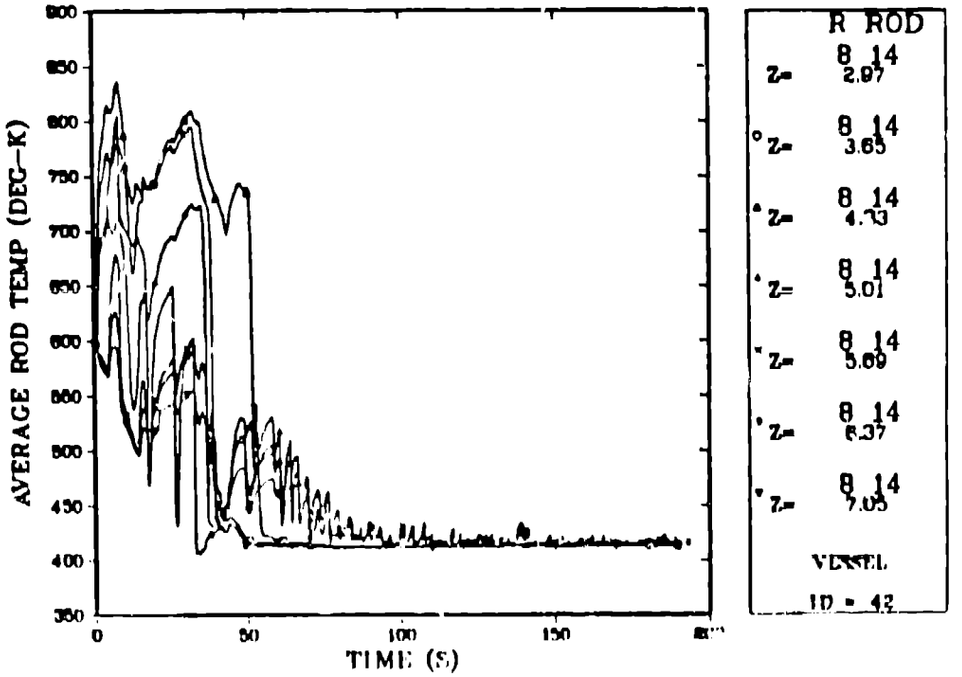

Figure 9. Rod 14 average rod cladding temperature history.

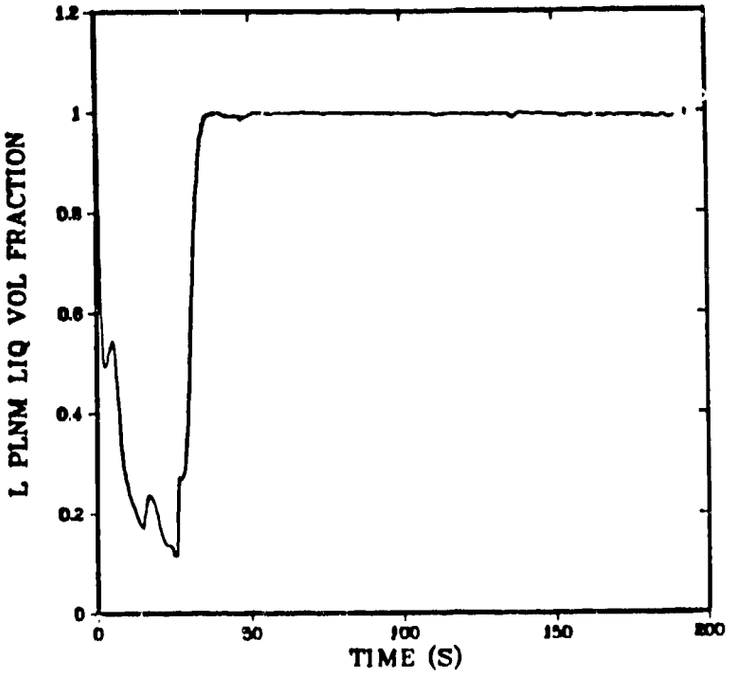

Figure 10. Lower plenum liquid volume fraction.

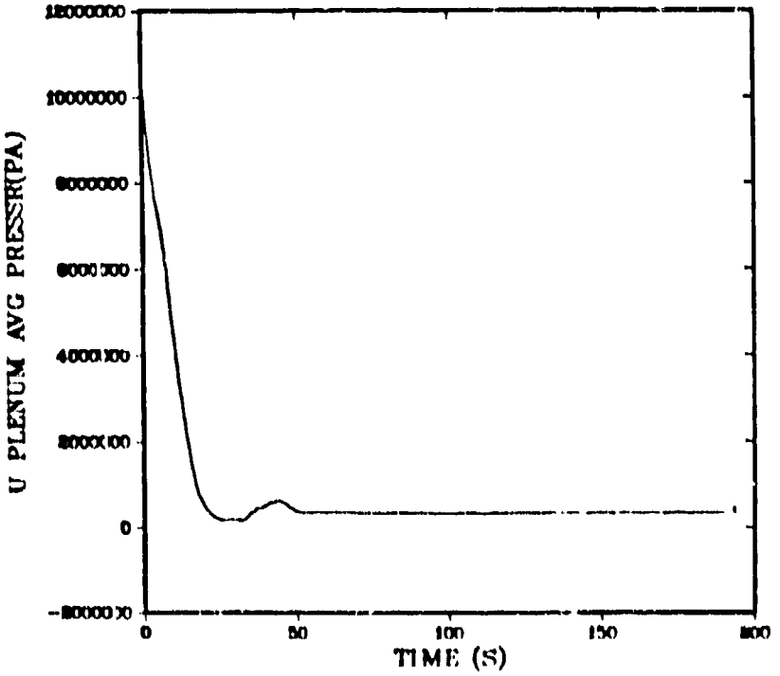

Figure 11. Upper plenum average pressure.

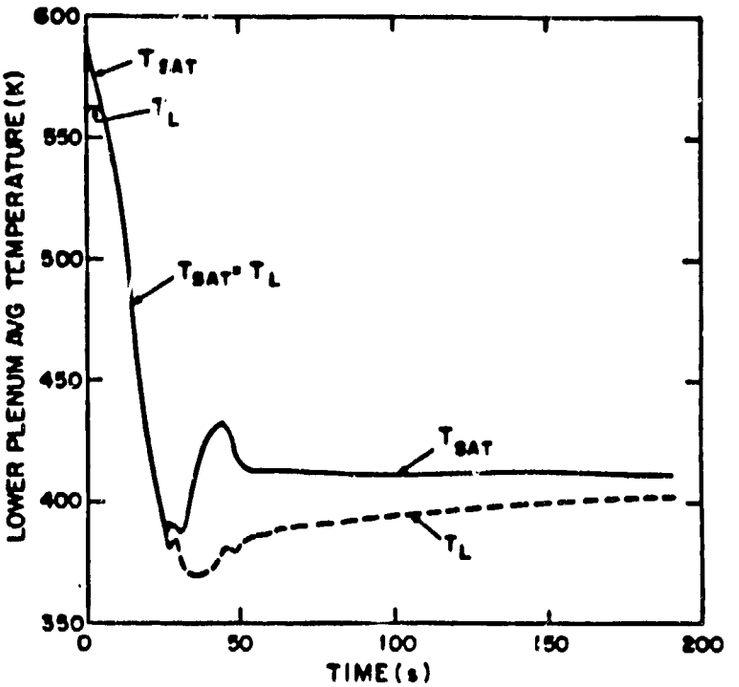

Figure 12. Lower plenum average liquid and saturation temperatures.

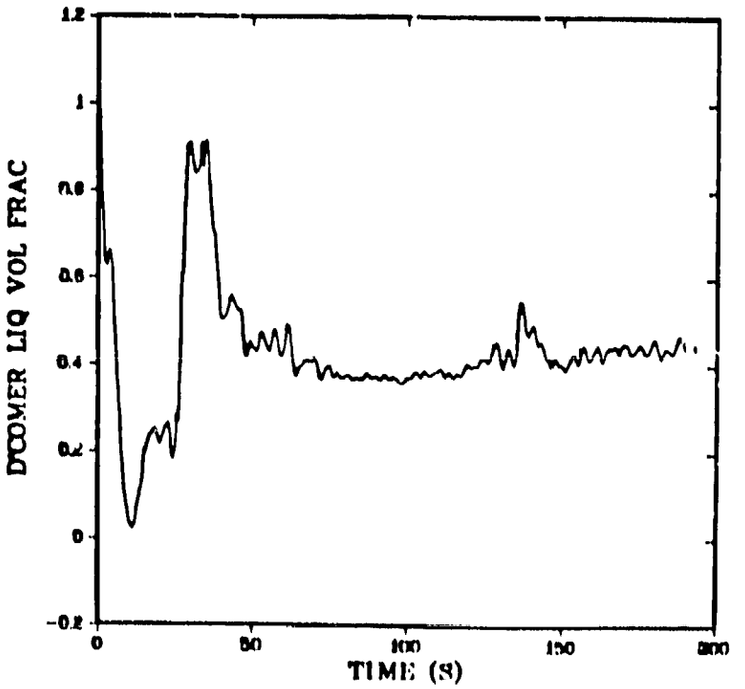

Figure 13. Downcomer liquid volume fraction.

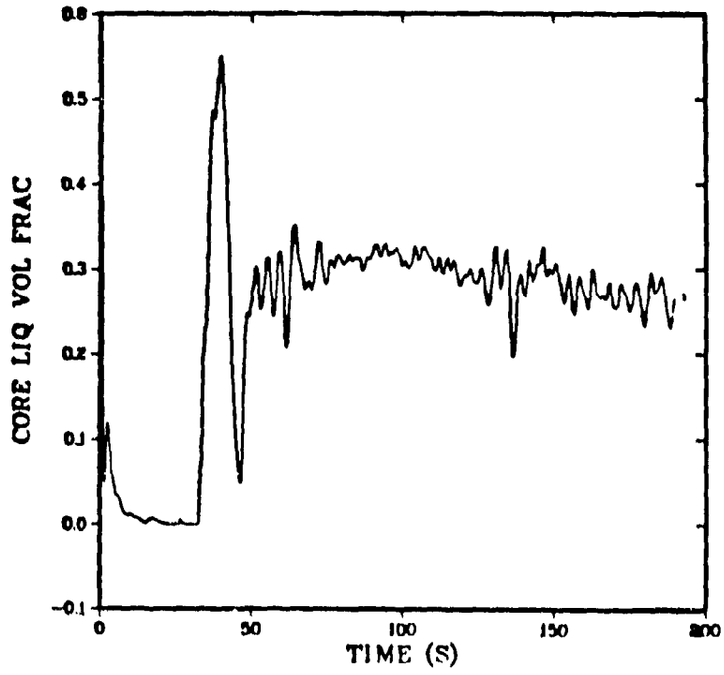

Figure 14. Core liquid volume fraction.

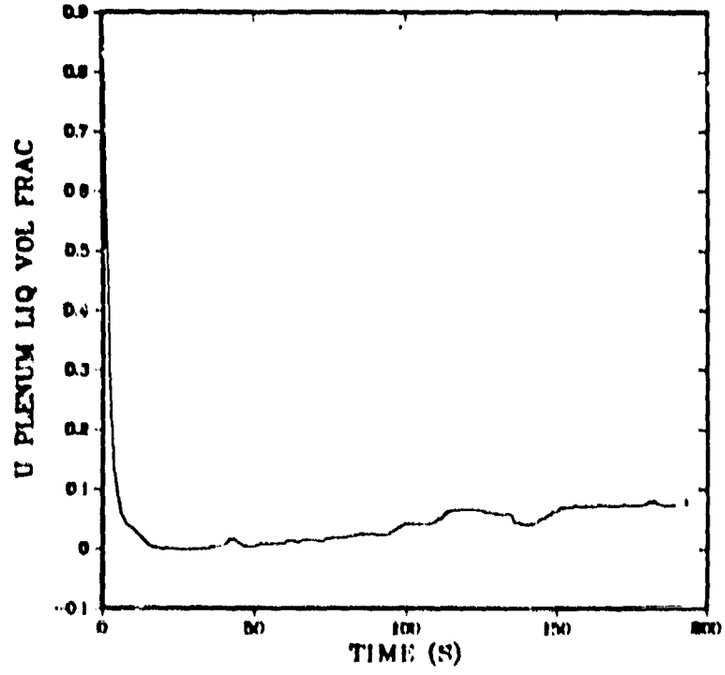

Figure 15. Upper plenum liquid volume fraction.

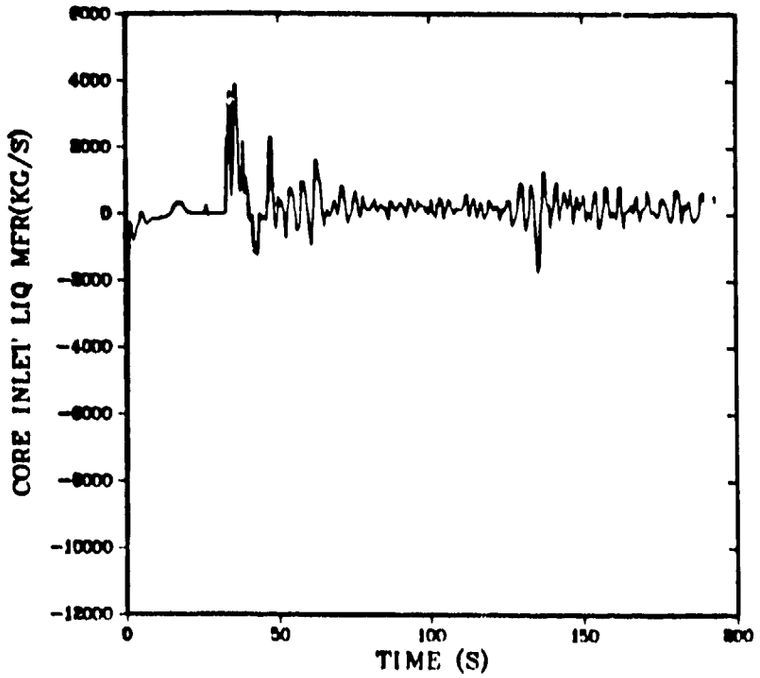

Figure 16. Core inlet liquid mass flow rate.

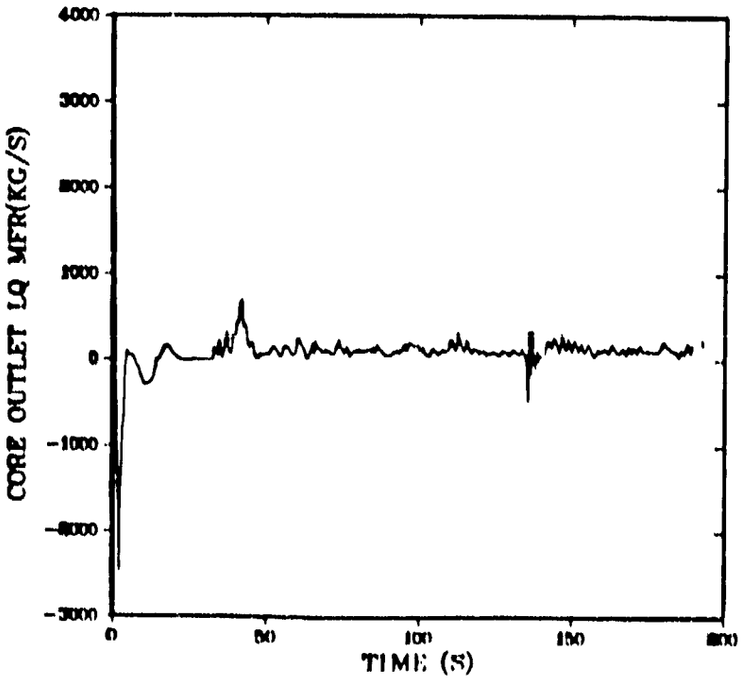

Figure 17. Core outlet liquid mass flow rate.

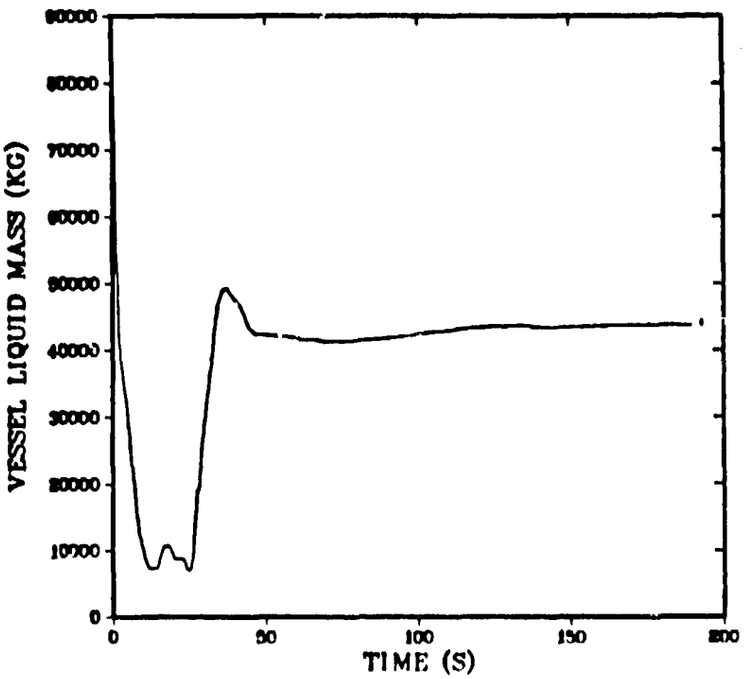

Figure 18. Vessel liquid mass.

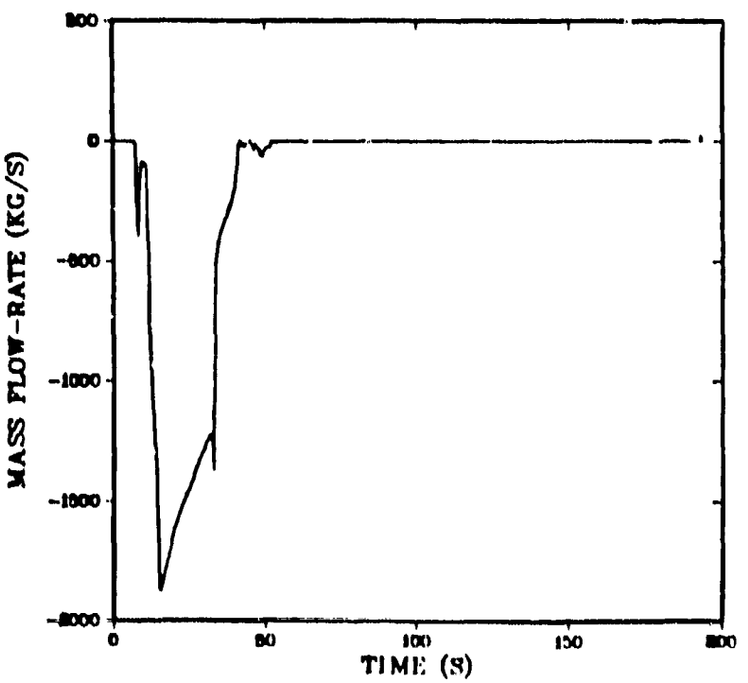

Figure 19. Accumulator mass flow rate (one loop only).

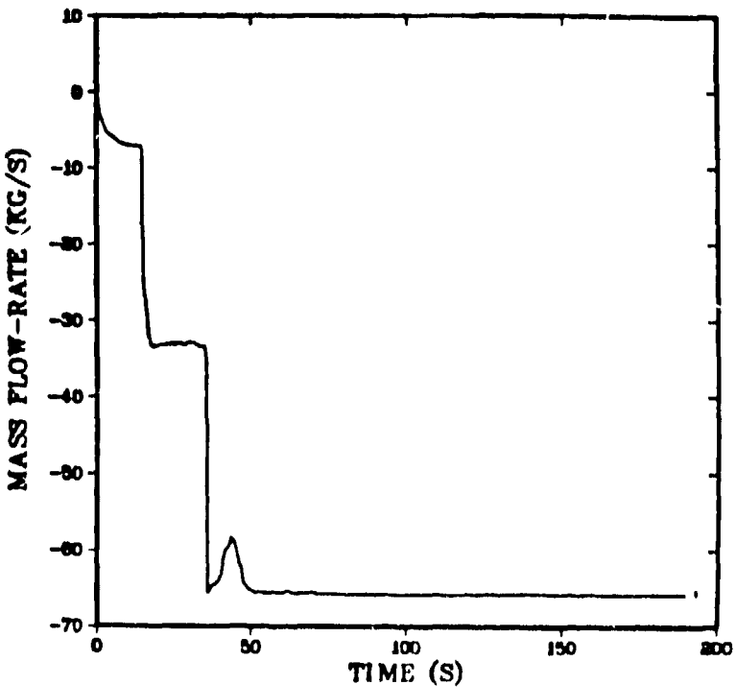

Figure 20. HPIS-LPIS flow rate (one loop only).

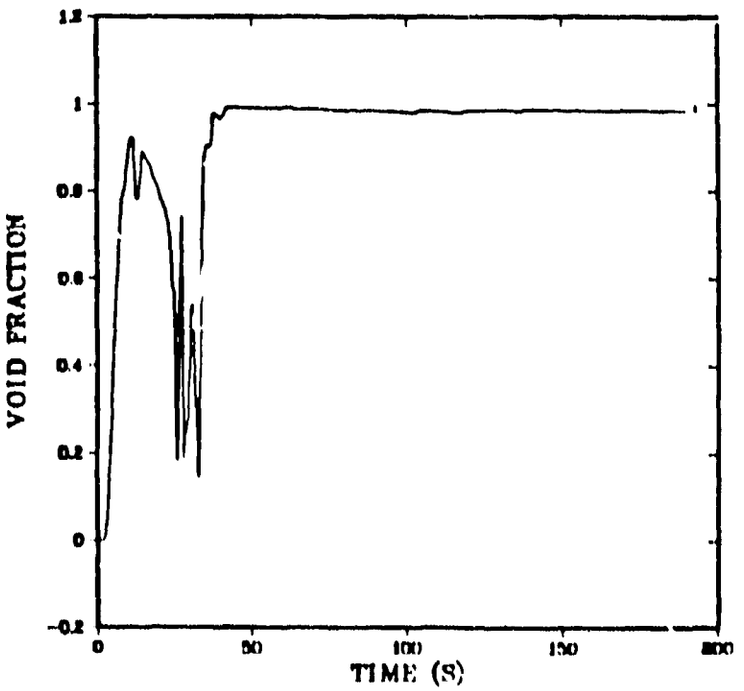

Figure 21. Intact-loop cold-leg void fraction.

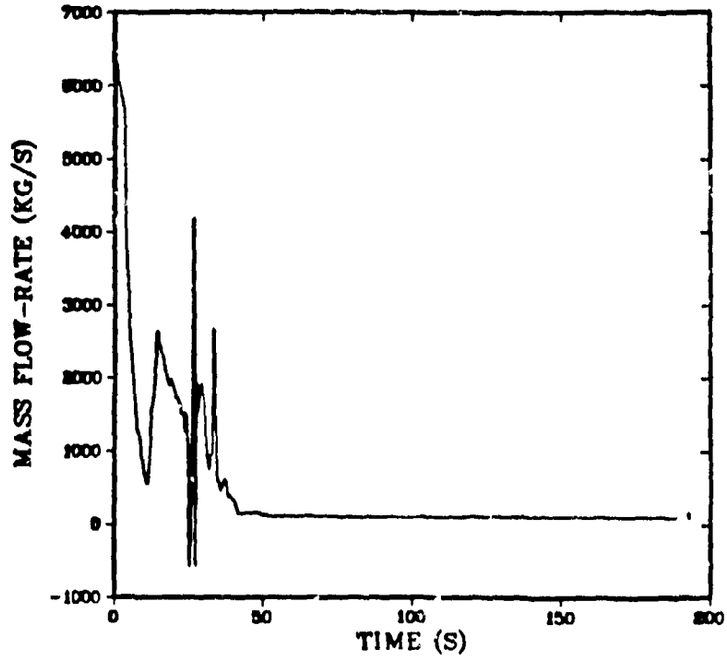

Figure 22. Intact-loop cold-leg mass flow rate.

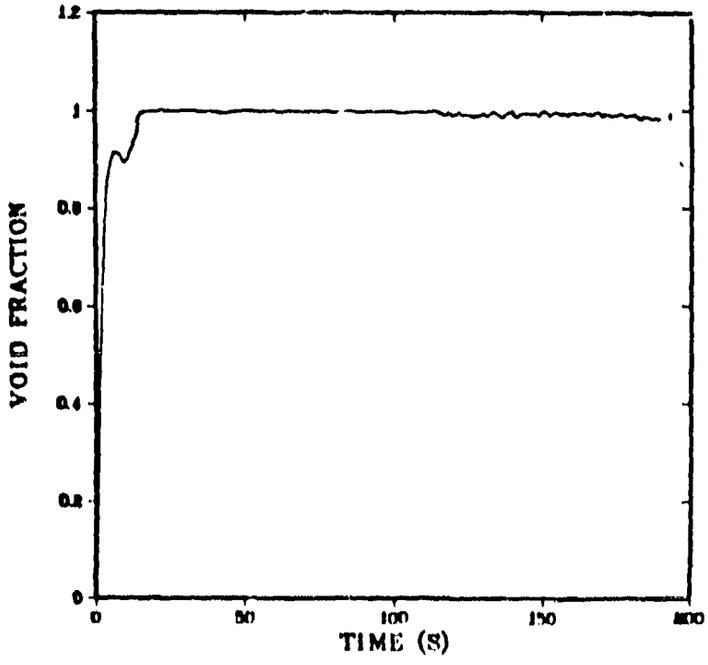

Figure 23. Intact-loop hot-leg void fraction.

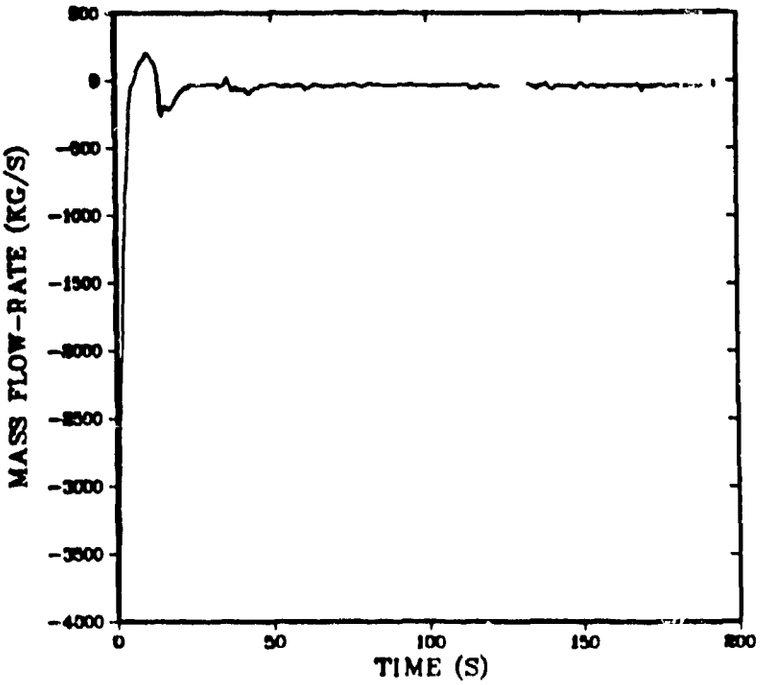

Figure 24. Intact-loop hot-leg mass flow rate.

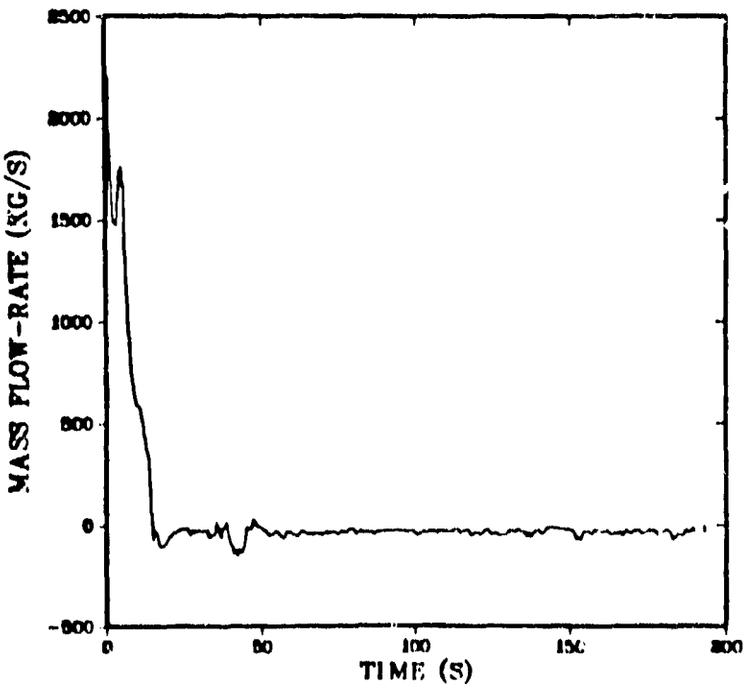

Figure 25. Pressurizer-loop hot-leg mass flow rate.

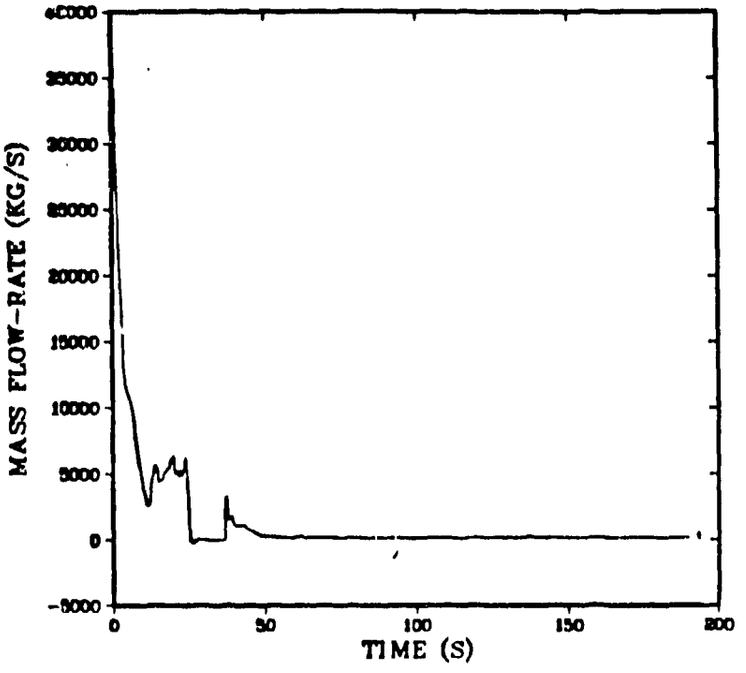

Figure 26. Vessel-side break mass flow rate.

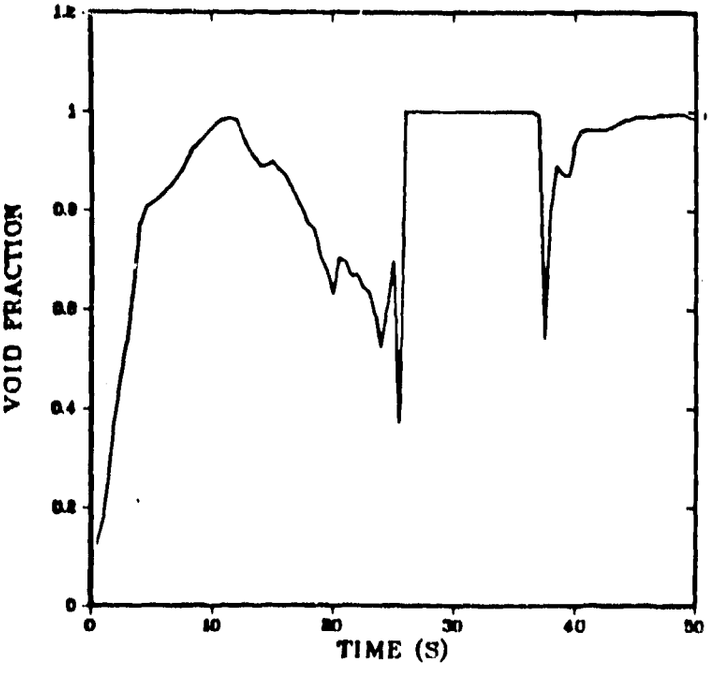

Figure 27. Broken cold-leg void fraction.

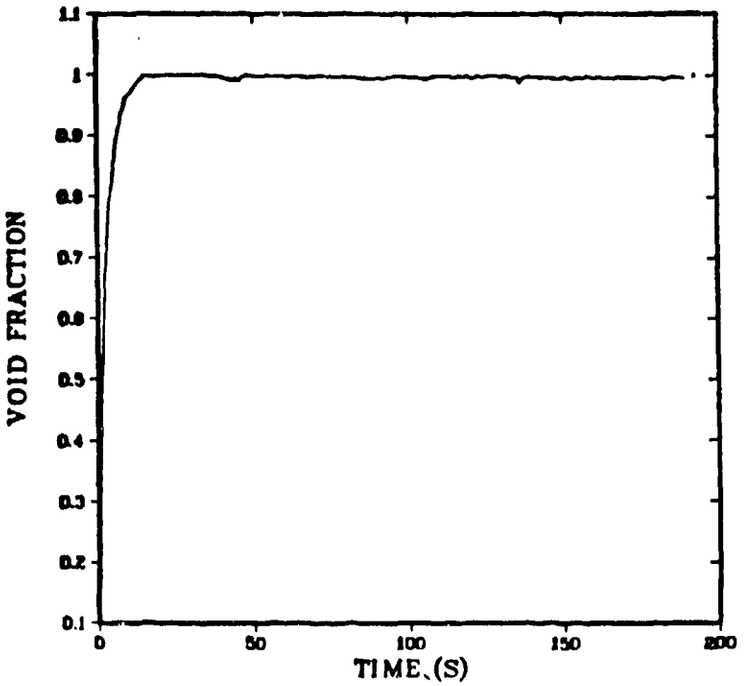

Figure 28. Broken-loop hot-leg void fraction.

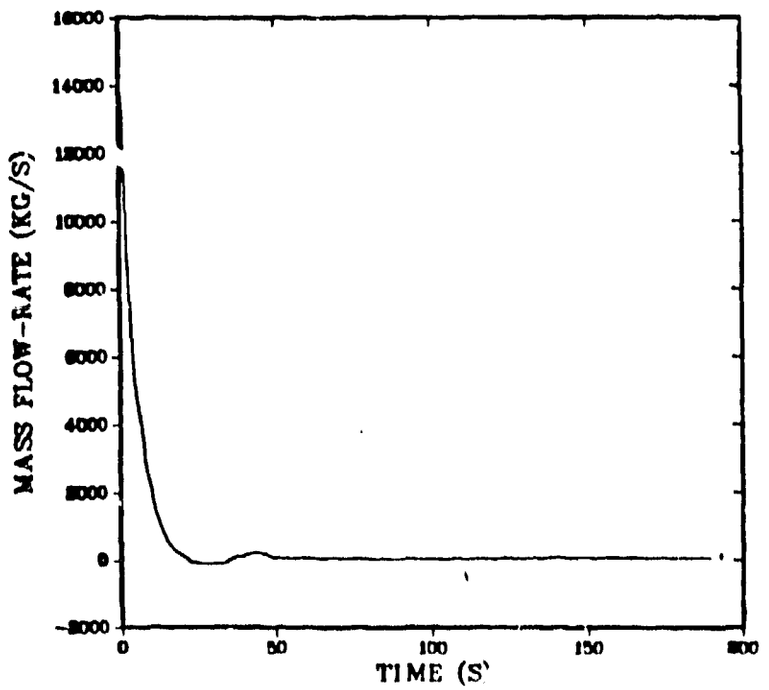

Figure 29. Broken-loop hot-leg side mass flow rate.

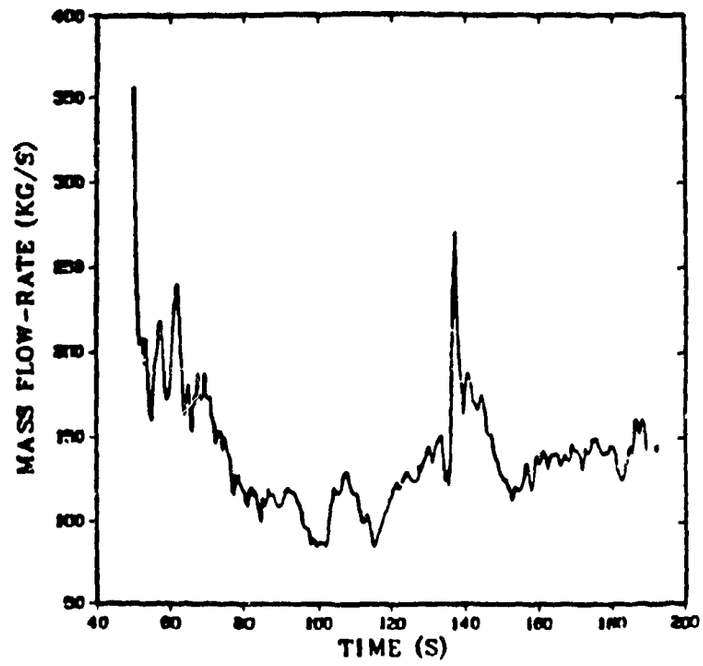

Figure 30. Broken cold-leg mass flow rate (positive flow out of vessel) during reflood.